ADVANCED INTELLIGENT SYSTEMS
Open Access
www.advintellsyst.com

Current-Limiting Control Strategies in Variable Capacitance Electrostatic Energy Harvesters

*Alireza Jalaliankhakshour, Gianluca Rizzello, Antonello Cherubini, Marco Fontana, and Giacomo Moretti**

Electrostatic energy harvesters (EEHs), especially those employing electroactive polymers, show significant potential to be scaled up into real-world technologies for ambient energy harvesting. Conventional EEH cycles involve rapidly charging and discharging a variable capacitor at specific instants corresponding to maximum and minimum capacitance values. This approach poses two major challenges in practical operation: 1) the precise detection of these extrema is difficult under stochastic inputs and 2) instantaneous charging demands high peak currents and power, creating significant cost and complexity burdens for large-scale applications. This work proposes control strategies that enable charging and discharging under stochastic excitations while also evaluating the impact of limiting the peak current on the maximum convertible energy. Traditional peak-triggered controls are compared with newly proposed smooth current control methods that use continuous AC-like driving voltages, whose phase is bound to the capacitance. Modeling and results on elastomeric generators show that smooth voltage controls can be implemented in a real-time prediction-free fashion, while competing in performance with peak-triggered controls even under realistic stochastic ambient energy harvesting conditions.

1. Introduction

Variable capacitance electrostatic generators lend themselves to a broad variety of layouts, which make them promising candidates for applications at different scales. Whereas micrometer-scale electrostatic energy harvesters (EEHs) have been proposed as a solution for energy recovery from vibrations,[1,2] in the past two decades, macroscale electrostatic generators have emerged, which might represent a promising option for large-scale renewable energy harvesting.[3] To comply with applications at different scales, EEHs rely on different embodiments. At the small scale, microelectromechanical system (MEMS) EEHs rely on parallel plate capacitor architectures with variable gaps.[4] Those architectures are unsuitable for upscaling, because of the limited ability of thick air gaps to tolerate high electric fields.[5] Macroscale generators have thus been developed using deformable dielectrics with high breakdown strength. The most popular class of such devices is the so-called dielectric elastomer generators (DEGs), which consist of stretchable dielectric rubbers covered with deformable electrodes.[6] DEGs have reached cyclic energy densities up to hundreds of J kg^{-1};[7] they have been experimentally demonstrated at scales ranging from millimeters to meters,[8] with a focus on small-to-medium-scale applications such as energy harvesting from human motion.[9] Moreover, remarkable effort has been put into understanding the feasibility of scaling DEGs up to multimeter scales for ocean wave energy harvesting.[3,10,11] Recently, dielectric fluid generators have been proposed,[12–14] which achieve capacitance variations by means of a relocation of dielectric fluid within dielectric pouches coated by compliant electrodes, featuring a structure similar to that of so-called hydraulically amplified self-healing electrostatic (HASEL) actuators.[15] Dielectric fluid generators provide a potentially promising solution to overcome some of the limitations of DEGs, e.g., the high sensitivity to dielectric breakdown of elastomeric materials upon cyclic loading.[16]

Developing large EEHs or clusters of harvesters to reach large-scale power production[3] is regarded as a strategic target by agencies working in the field of renewable energy harvesting, especially wave energy conversion.[17–19]

EEHs rely on a cyclic working principle, and their operation involves high voltages (especially at macroscopic scales) to achieve high electric fields. EEHs' control involves cyclically charging (i.e., priming) and discharging the harvester capacitor based on the current capacitance values. Because this operation involves bidirectional energy fluxes, dedicated electronic solutions are required to manage the energy generated by EEHs.

A. Jalaliankhakshour, A. Cherubini, G. Moretti
Department of Industrial Engineering
University of Trento
Via Sommarive 9, 38123 Trento, Italy
E-mail: giacomo.moretti@unitn.it

G. Rizzello
Department of Systems Engineering
Saarland University
c/o ZeMA, Eschberger Weg 46, Gewerbepark, Gebäude 9, 66121 Saarbrücken, Germany

M. Fontana
Institute of Mechanical Intelligence
Scuola Superiore Sant'Anna
Via L. Alamanni 13B, 56010 Pisa, Italy

The ORCID identification number(s) for the author(s) of this article can be found under https://doi.org/10.1002/aisy.202500985.

DOI: 10.1002/aisy.202500985

At small scales, circuits based on charge pumps,[20] electrets,[21] or self-priming topologies[22] have been proposed. At large scales, however, high efficiency and the ability to effectively regulate the voltage to maximize the energy yield are key, and bidirectional DC–DC converters are thus required.[23–25]

It is well-known that, to maximize the convertible energy in the presence of a given motion pattern, charging and discharging should take place at fixed configurations, i.e., respectively when the EEH capacitance is maximum/minimum.[1,26] In a practical context, where the capacitance changes continuously with time, this corresponds to charging/discharging the EEH in a short time.

To achieve this, the power converter should be able to provide peak currents and powers (for charging/discharging) much higher than the average current/power produced in a working cycle. This would in turn affect the rated power of the switching components and, ultimately, the price and size of the power converter.[27] Identifying trade-offs between high-rated currents and the ability to implement high-yield working cycles is a highly relevant question for large-scale EEH applications. Nonetheless, only a few works have investigated the implications of limiting the charging currents on the performance of EEHs[28] and, to our best knowledge, no systematic investigations of the implications of different current limitations on the maximum convertible energy have been produced up until now.

This study presents an analysis of control strategies to limit the peak current in EEHs and analyzes their impact on the maximum energy conversion capability. We present a comparative analysis of two different control approaches, namely, 1) peak-triggered controls, which involve charging/discharging in a finite amount of time using specific conditions (e.g., detection of peaks in capacitance/displacement) as trigger events, and 2) quadrature controls, which involve applying smooth voltage profiles in phase quadrature with the variable capacitance profile. While peak-triggered controls have been used in practical applications, including real-time settings,[11] quadrature controls are introduced here for the first time. We show that this latter class of controls leads to higher convertible energy than peak-triggered controls in the presence of strong limitations on the peak current. While, in principle, generating quadrature voltage profiles implies predicting the EEH displacement (or capacitance), we propose a prediction-free online implementation for quadrature controls with real-time capability. The method relies on an observer-like filter that continuously provides a normalized estimate of the time derivative of the EEH capacitance, which is then used to generate the quadrature voltage driving signal.

We present a validation/demonstration of the proposed control strategies on an archetypal prototype of an EEH, consisting of an elastomeric variable capacitor. Our proposed control strategies reach performance that closely matches theoretical expectations, and are applicable in the presence of multiharmonic capacitance variations. With respect to previous simulation works that investigated the implications of restricting the peak current in EEH generation cycles,[28] this work presents a systematic theoretical and experimental analysis of the implications of current limitations on the maximum convertible energy. With respect to previous works that used smooth voltage profiles (e.g., alternated current driving) through specific circuit topologies,[29] this work investigates strategies that are circuit independent and are potentially applicable through DC–DC converters, relevant for large-scale EEH systems.

The rest of the study is structured as follows. Section 2.1.1 presents an overview of EEH working cycles and introduces peak-triggered and quadrature control strategies. Section 2.2 presents a theoretical analysis and simulation results for different control strategies. Section 2.3 presents an open-loop experimental validation and comparison of the different control strategies. Section 2.4 introduces online prediction-free implementations of the proposed approaches and presents their experimental validation. Section 2.5 reports a discussion of advantages and limitations of the porposed control strategies. Section 3 presents the conclusions.

2. Results and Discussion

2.1. Working Cycles and Current Limitation Strategies

2.1.1. EEH Working Cycles

EEHs leverage variations in capacitance imposed by an external mechanical energy source and voltage modulation applied through a control strategy to cyclically convert mechanical work into electrical energy.

The prototypical control of EEHs follows a working cycle that consists of a sequence of four operations (**Figure 1**A): 1) The EEH is initially uncharged, and it is mechanically deformed from a configuration 1 with minimum capacitance to a configuration 2 with maximum capacitance; 2) When the generator reaches maximum capacitance, the EEH is charged to a target voltage (configuration 3). This priming phase involves an amount of electrical energy to be initially spent; 3) While the device capacitance decreases, a voltage difference is applied on the electrodes of the harvesters, and electrostatic forces do work against the mechanical forces that drive the deformation. In this generation phase, electrical energy is positively generated at the expense of mechanical work done on the system by the external force; 4) As the EEH capacitance reaches again its minimum (configuration 4, the capacitor is discharged, the stored electrical energy is recovered, and the cycle is restarted.

The voltage signal applied during the generation phase 3-4 can be modulated according to different control strategies (constant charge, constant voltage, constant field, etc.).[1,2,30] Here, we make reference to a constant-voltage control (Figure 1B): the value of the applied voltage is held constant (say, V_0) during the generation phase, and a current is delivered by the EEH to the driving electronics as a result of the progressive decrease in capacitance. While harvesters based on stretchable polymers (DEGs) achieve maximum convertible energy density if operated at a constant electric field,[6,26] constant-voltage control is a popular choice in different classes of electrostatic devices. These include EEHs based on a sliding plate topology (e.g., comb drive MEMSs),[31,32] in which the distance between the capacitor plates remains constant upon deformation, and dielectric fluid generators featuring a variable fluid gap (also called HASEL generators), in which the maximum working voltage is set by the thickness of the solid dielectric layers (constant throughout operation).[12–14,33] In an ideal setting, charging and discharging

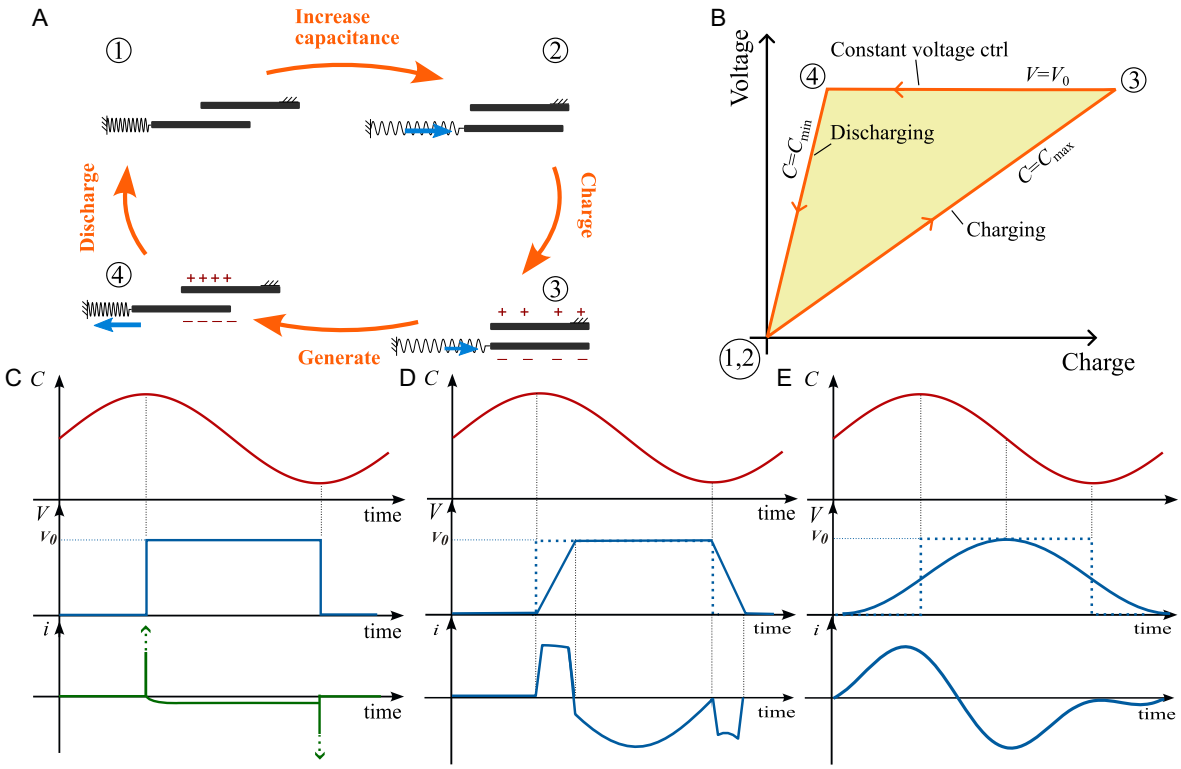

Figure 1. A) Four-phase working cycle of a generic EEH. Reference is made to a parallel plate capacitor for the sake of illustration. B) Charge–voltage trajectory for a working cycle of an EEH controlled according to a constant-voltage strategy. This strategy prescribes that the applied voltage is held constant during the generation phase, while the capacitance is decreasing. C–E) Qualitative time profiles of the voltage V and current i for different control strategies, given a same (smooth) profile for the capacitance C. (C) Ideal cycle (instantaneous charging/discharging); (D) peak-triggered control; (E) quadrature control.

happen instantaneously, i.e., the capacitance does not sensibly change during those phases. As a consequence of that, the ideal representation of a constant-voltage generation cycle on a charge-voltage diagram[2] consists of a triangular trajectory (as in Figure 1B), where isocapacitance lines 1–2 and 3–4 represent the priming and discharging phases, respectively. In applications, the EEH is coupled with a mechanical system or an oscillator excited by external forces; therefore, its capacitance varies continuously in time (Figure 1C). In these conditions, implementing the ideal cycle defined in Figure 1B is only possible if the voltage is instantaneously raised from 0 to V_0 (priming), and then instantaneously removed during discharging. This requires very high (theoretically infinite) currents that 1) are practically upper bounded by the rating of the power electronics and 2) would cause significant dissipation. For instance, when a voltage step is applied to a series RC set, the energy dissipated on the resistance equals that delivered to the capacitor.

2.1.2. Current Limitation Strategies

We hereby analyze two alternative approaches to limit the working current in EEHs and investigate their implication in terms of energy yield.

A practical strategy, hereafter referred to as "peak-triggered control," consists of starting charging (discharging) when the capacitance reaches a maximum (minimum) and completing it in a finite amount of time (Figure 1D). This strategy is representative of solutions used in the practice so far,[11] and it can be implemented either by keeping the current constant during charging/discharging,[28] using predefined voltage rise/decrease profiles, or passing the ideal step voltage profiles through a low-pass filter. In the remainder of the article, we will refer to linear time ramps for voltage increase/decrease. This strategy can be implemented in a causal fashion (without a priori knowledge of the capacitance profile), and it only requires detecting maxima/minima in capacitance (or directly related measurable variables, e.g., displacements). The maximum current requested in this case depends on the charging time (the slope of the prescribed voltage ramp) and the harvester capacitance during charging.

A second possibility proposed here and referred to as "quadrature control" consists of the application of a smooth voltage waveform (e.g., a sinusoidal or other smooth voltage profile) with a phase delay of 90° (a quarter of period) with respect to the capacitance waveform (Figure 1E), i.e., the voltage reaches a maximum (minimum) when the capacitance is halfway on its decrease (increase) path. This control strategy does not rely on a distinct sequence of operations, as it uses a smooth, continuously varying voltage. Nonetheless, it still enables positive generation as it provides the EEH with a lower average voltage during the capacitance increase phases and a higher voltage during the capacitance decrease.

Compared to a peak-triggered control, the quadrature control relies on waveforms that are in phase with (and represent a

smoothed version of) the square voltage pulse applied in the ideal cycle (Figure 1D). However, it requires a priori knowledge of the capacitance waveform (to determine the quadrature phase), which might not be available in applications where the harvester is subject to random excitation.

2.2. Theory and Numerical Results

With the aim of comparing peak-triggered and quadrature control, and establishing limits in terms of their resulting convertible energy, we refer to a generic EEH whose capacitance periodically varies between $C_{\min}$ and $C_{\max}$ in a prototypical working cycle with period T. We denote V_0 as the maximum working voltage (e.g., the high-voltage value in a constant-voltage control). We introduce the following dimensionless quantities

$$V^* = \frac{V}{V_0},\ C^* = \frac{C}{\Delta C},\ q^* = \frac{q}{\Delta C V_0}$$
$$t^* = \frac{t}{T},\ i^* = \frac{Ti}{\Delta C V_0},\ \mathcal{E}^* = \frac{\mathcal{E}}{\Delta C V_0^2} \tag{1}$$

where the asterisk $(\cdot)^*$ denotes the dimensionless form of a generic variable, $\Delta C = 0.5(C_{\max} - C_{\min})$ is the amplitude of the capacitance fluctuations between its limit values, V is the voltage difference on the EEH, q is the charge, i is the current, and $\mathcal{E}$ is the energy generated in a period/cycle.

We evaluated the theoretical limit performance of different current limiting control strategies assuming sinusoidal temporal variations of the EEH capacitance: $C^* = C_b^* + \cos(2\pi t^*)$, with $C_b^* = (C_{\max} + C_{\min})/\Delta C$. For peak-triggered control (**Figure 2**A), we considered linear voltage ramps for charging/discharging, whose durations cover different fractions t_r^* of the period. For quadrature control (Figure 2B), we modulated the shape of the voltage waveform using a smooth square-to-sine transition function. The applied voltage signal was defined as

$$V(t) = \frac{V_0}{2}\left[1 + \frac{1}{\arctan(1/N)} \cdot \arctan\left(\frac{\sin(2\pi t/T)}{N}\right)\right] \tag{2}$$

where N is a dimensionless shape factor that governs the waveform profile. For $N \ll 1$, the function approximates a square wave with sharp transitions, while $N \gg 1$ progressively smoothens the waveform into a sinusoidal shape.

In order to quantify the theoretical reduction in energy yield (with respect to an ideal cycle) due to current limitations, we neglected any leakage effects and dynamics and evaluated the energy converted per period and the instantaneous current, $i = d(CV)/dt$, as a result of the prescribed voltage waveforms.

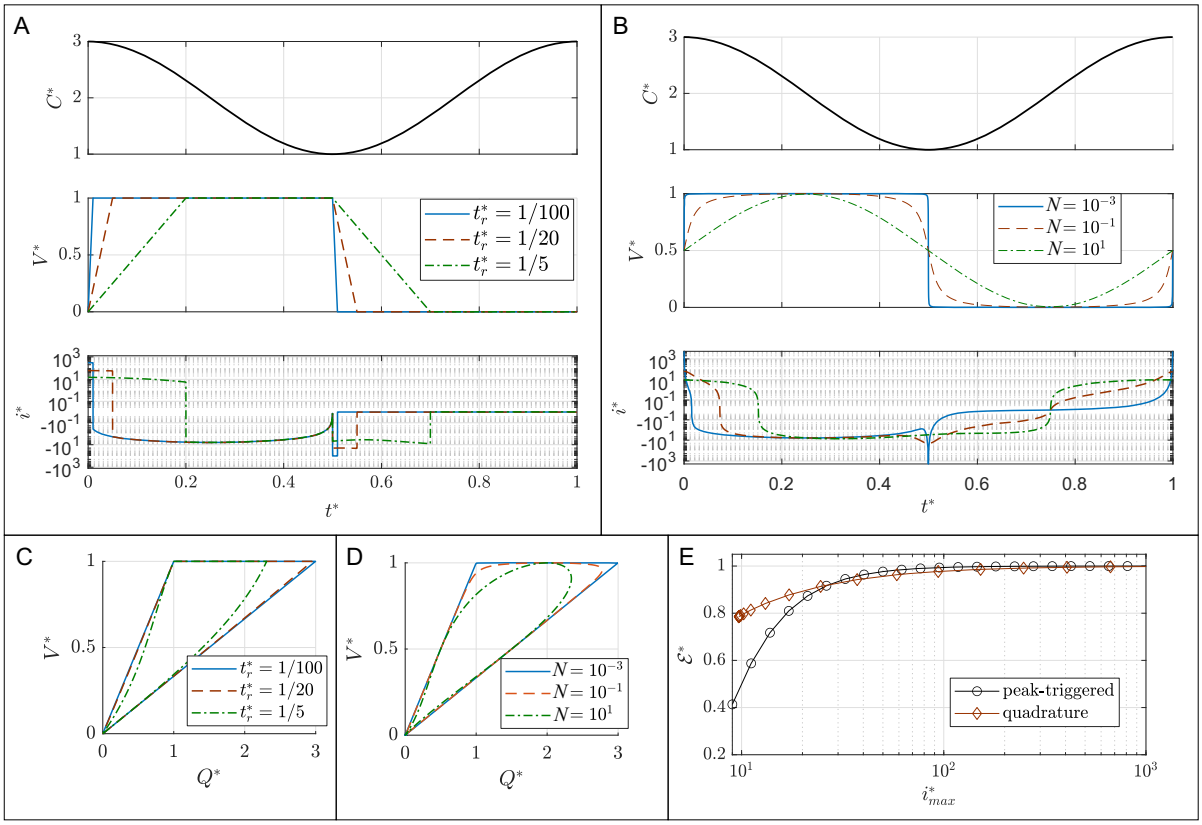

Figure 2. Theoretical comparison of peak-triggered and quadrature control for a generic variable capacitance generator. A,B) Time series of the EEH capacitance, applied voltage, and resulting current (on a logarithmic y-scale) for peak-triggered control with different rising times (A) and quadrature control with different smoothing factors (B). C,D) Voltage–charge trajectories for peak-triggered (C) and quadrature (D) control, associated with (A) and (B) respectively. E) Theoretical energy generated as a function of the peak current for the two controls. For the conducted analysis, a bias capacitance equal to $C_b^* = 2$ was assumed, and no resistive dissipation was considered.

In the case of peak-triggered control, varying t_r^* from 0.01 to 0.2 leads to a reduction in the peak current of more than two orders of magnitude (Figure 2A). For quadrature control (Figure 2B), a sinusoidal voltage waveform ($N > 10$) results in a peak current lower (≈35% less) than that obtained with a peak-triggered control with $t_r^* = 0.2$. Both controls result in voltage-charge trajectories (Figure 2C,D) that are strictly enveloped by the triangular trajectory generated by an ideal cycle (see Figure 1B), hence resulting in a reduction in the theoretically generated energy (Figure 2E). The maximum energy that can be converted in a constant-voltage cycle is given by $\varepsilon = \Delta C V_0^2$ (i.e., the area of the resulting triangular cycle on a Q–V diagram), which becomes $\mathcal{E}^* = 1$ in dimensionless coordinates (see Equation (1)). Increasing the charging time t_r (and, hence, decreasing the peak current i_{max}) leads to an indefinite reduction in the energy generated through a peak-triggered control, whereas increasing N indefinitely toward a quadrature control (i.e., using a sinusoidal voltage) leads to a finite positive generated energy. For low dimensionless values of the peak current, below 30, the energy generated via a quadrature control is higher (up to roughly two times) than that obtained with a peak-triggered control using the same peak current (Figure 2E). The energy generated via a quadrature control in the presence of sinusoidal capacitance variations and quadrature sinusoidal voltage profiles ($N \gg 1$) is ≈0.79 times that obtained through a theoretical ideal cycle (squarewave voltage profile). This can be motivated analytically by observing that, in a limit quadrature cycle (with $N \to +\infty$, $V(t) \to 0.5V_0(1 + \sin(2\pi t/T))$)

$$\varepsilon^* = -\oint V\mathrm{d}q = -\oint \frac{V^2}{2}\mathrm{d}C = -\int_0^T \frac{V^2}{2}\dot{C}\mathrm{d}t = \frac{\pi}{4}\frac{\Delta C V_0^2}{T}\int_0^T \left[1+\sin\left(\frac{2\pi}{T}t\right)\right]^2 \sin\left(\frac{2\pi}{T}t\right)\mathrm{d}t = \frac{\pi}{4}\Delta C V_0^2 \tag{3}$$

leading to $\mathcal{E}^* = \pi/4 \simeq 0.785$. This result means that driving the EEH with a quadrature sinusoidal waveform (with a phase delay of 90° with respect to the externally applied sinusoidal capacitance variation) leads to a moderate decrease in performance (on the order of 21%), while limiting the peak current by more than two orders of magnitude compared to a nearly-ideal peak-triggered control with fast charging–discharging ($t_r^* = 0.01$).

2.3. Experimental Validation

To validate the theory, we performed tests on a stretchable capacitor, namely a DEG. The DEG consisted of a single layer of stretchable silicone dielectric, coated by compliant electrodes and clamped at the ends (**Figure 3**A). The DEG was subjected to cyclic stretching in one direction, reaching maximum capacitance in correspondence with the maximum applied stretch. With the aim of isolating the current contributions due to capacitance variations (while rejecting spurious effects due to leakage currents or charge dispersion), and hence validating the theoretical observations of Section 2.2, we carried out the tests at relatively low voltages/electric fields (1 kV, over an initial DEG thickness of 145 μm).

We ran experiments in which we applied sinusoidal elongations at 1 Hz to the DEG sample and controlled the applied voltage in an open-loop fashion (based on the prescribed position profiles), applying trapezoidal voltage profiles (peak-triggered control) and smooth voltage profiles, as given by Equation (2) (quadrature control). In contrast with the theoretical formulation (Figure 2), where sinusoidal capacitance temporal profiles were assumed, here we ran the tests with an applied sinusoidal variation of the DEG length, which possibly resulted in capacitance profiles that slightly deviated (at the second order) from a sinusoidal waveform. Despite that, the generated energy as a function of the measured peak current (Figure 3B) was found to follow a trend that is closely consistent with theoretical predictions, proving that the analyzed control strategies are robust against moderate variations of the capacitance waveforms. We confirmed that the peak current is significantly reduced through proper timing or waveform shaping. The energy generated by applying a sinusoidal quadrature voltage is on the order of 80% of that generated by applying squarewave profiles (as expected from the theory) that would result in peak currents several orders of magnitude higher. The resulting decrease in the measured generated energy $\mathcal{E}$ with respect to the maximum theoretical value $\mathcal{E}_{max}$ (calculated from the maximum/minimum values of the DEG capacitance during deformation) is reported in **Table 1** for different values of the charging/discharging time t_r (peak-triggered control) and the smoothing exponent N (quadrature control).

The measured current profiles (Figure 3C,D), corresponding to different durations of the charging/discharging in peak-triggered control (Figure 3C), and different shape factors in quadrature control (Figure 3D), are consistent with the trends generated from the theory (Figure 2A,B). By decreasing the charging/discharging time, or as the applied voltage waveform approaches a squarewave, an increase in the current is observed.

The peak-triggered strategy demonstrates a steep rise in energy with increasing peak current, consistent with its aggressive charging dynamics. In contrast, the quadrature strategy maintains a nearly constant energy yield while significantly reducing the peak current. The lowest value of the peak current for the quadrature experiment is 3.2 μA, which leads to 0.16 mJ/cycle generated energy, as opposed to 0.1 mJ/cycle (37% less) for the theoretical value of the peak-triggered strategy with the same current.

2.4. Prediction-Free Online Implementation

In practical applications, such as energy harvesting from natural mechanical energy sources,[6] the profile of the input deformation (as well as the external excitation) of an EEH is not known a priori. In these situations, an online control strategy is necessary. Whereas peak-triggered control has been used in practical scenarios in the presence of stochastic excitation,[11] online application of quadrature control presents additional challenges, since guaranteeing the quadrature phase shift might, in general, require a prediction of the harvester deformation waveform. We hereby present a strategy for practical online implementation of the quadrature control, which is applicable when the spectrum of the EEH capacitance variation has a narrow bandwidth around the periodic signal carrier frequency. This reflects the case in which the capacitance signal is not an ideal sinusoid, but also exhibits slow fluctuations in amplitude and phase.

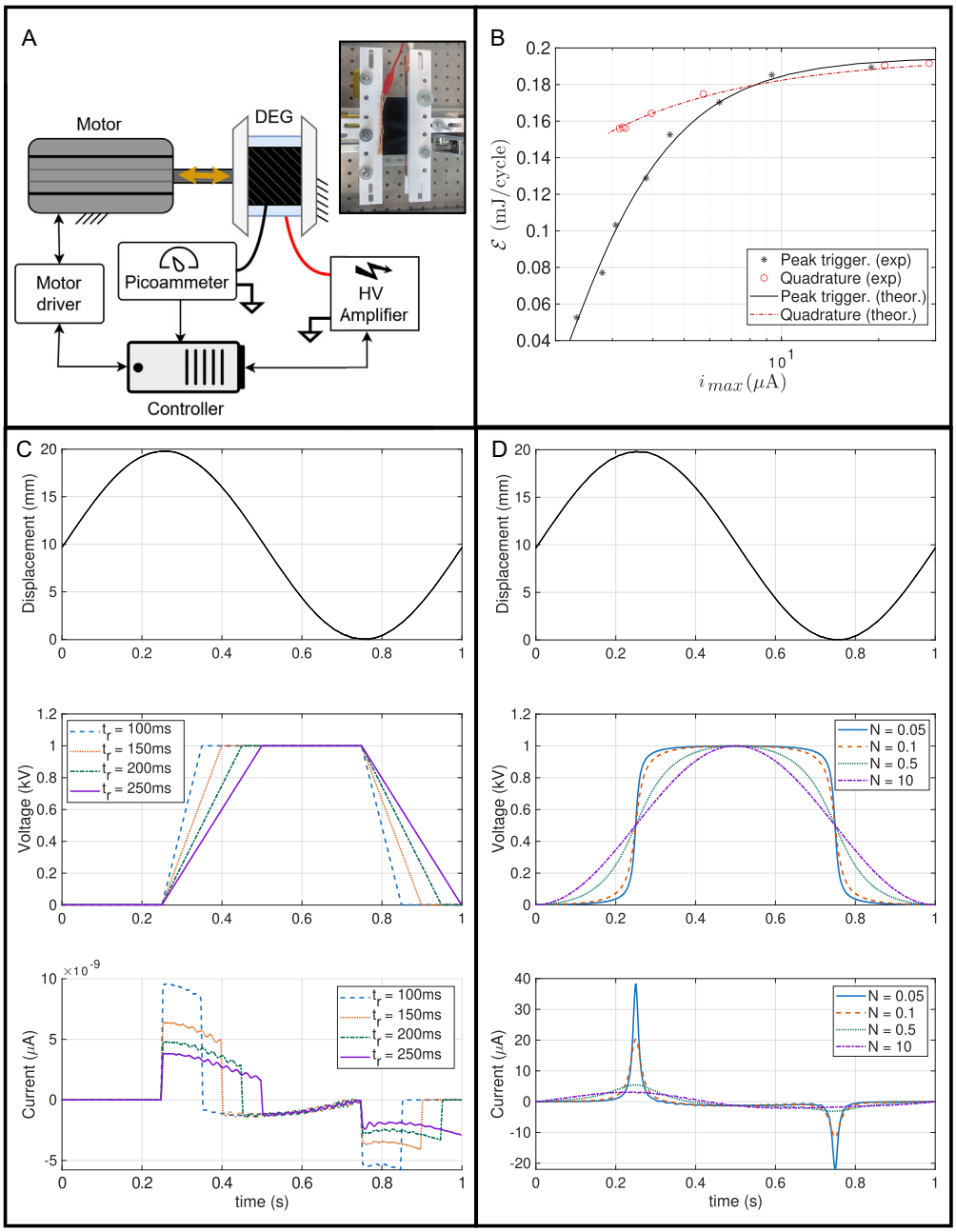

Figure 3. A) Experimental setup: a DEG sample is subjected to cyclic tensile stretching in the presence of a controlled applied voltage, and current is measured throughout the cycle. B) Measured generated energy as a function of the peak current, for peak-triggered and quadrature control. Markers represent experimental data, lines represent theoretical predictions based on the measured maximum/minimum capacitance. C,D) Time series of the sample displacement, applied voltage, and measured current for open-loop peak-triggered (C) and quadrature (D) control.

Implementations of both peak-triggered and quadrature control can be devised by relying on real-time measurements of the time derivative of a control signal $y(t)$, which represents either the EEH capacitance or displacement. The estimated derivative $\hat{\dot{y}}(t)$ can be used to 1) identify trigger time instants for charging/discharging (using zero crossings of $\hat{\dot{y}}(t)$) or 2) build quadrature voltage waveforms. Provided that the capacitance has the same monotonicity as $y(t)$, quadrature voltage waveforms should be in-phase with $-\hat{\dot{y}}(t)$, and they should vary between 0 and a target voltage V_0. Such quadrature waveforms can be built by normalizing $\hat{\dot{y}}(t)$, which involves predicting in real time the amplitude of the signal oscillations.

Whereas estimates of $\hat{\dot{y}}(t)$ could be obtained from direct computation using measurements of $y(t)$, such a direct computation would not provide a straightforward manner to normalize $\hat{\dot{y}}(t)$ for quadrature control, and it would be prone to inaccuracies due to

Table 1. Percentage loss of generated energy ε relative to the ideal constant-voltage energy ε_{max} for a) peak-triggered and b) quadrature control.

a) Peak-triggered control	
t_r [ms]	$\frac{\varepsilon_{max}-\varepsilon}{\varepsilon_{max}}$ [%]
100	5.0
150	13
200	21
250	34
b) Quadrature control	
N	$\frac{\varepsilon_{max}-\varepsilon}{\varepsilon_{max}}$ [%]
0.05	2.6
0.1	2.4
0.5	10
10	20

noise, or time delays introduced by high-pass filters used in place of differentiators to reduce the noise.

To solve these problems, in the following, we propose a state observer-based approach that provides a real-time and delay-free reconstruction of the derivative of the input signal even in the presence of noisy measurements. It is assumed that $y(t)$ has a narrow spectrum and can be approximated through a biased sinusoidal function

$$y(t) = y_0 + y_1 \sin(\overline{\omega} t) \tag{4}$$

where y_0 is the mean value, y_1 is the amplitude, and $\overline{\omega}$ is the angular frequency of the base excitation, which is assumed to be known. Signal y in (4) can be generated as the output of the following autonomous linear system

$$\begin{cases} \dot{\mathbf{x}} = A\mathbf{x} \\ y = C\mathbf{x} \end{cases} \tag{5}$$

where

$$\mathbf{x} \in \mathbb{R}^3, \quad A = \begin{bmatrix} 0 & 0 & 0 \\ 0 & 0 & 1 \\ 0 & -\overline{\omega}^2 & 0 \end{bmatrix}, \quad C = [1 \quad 1 \quad 0], \quad \mathbf{x}(0) = \begin{bmatrix} y_0 \\ 0 \\ \overline{\omega} y_1 \end{bmatrix} \tag{6}$$

where the choice of initial condition $\mathbf{x}(0)$ ensures consistency of y with Equation (4). The time derivative of y can readily be obtained from $\mathbf{x}$, since

$$\dot{y} = C\dot{\mathbf{x}} = C_d\mathbf{x}, \quad \text{with} \quad C_d = CA = [0 \quad 0 \quad 1] \tag{7}$$

Computation of $\mathbf{x}$ via integration of (5) would require the knowledge of initial condition $\mathbf{x}(0)$, which is generally not available as y_0 and y_1 are unknown. Nevertheless, the structure of Equation (6) can still be used to build an observer that estimates $\mathbf{x}$ for any unknown initial condition $\mathbf{x}(0)$. Observability of Equation (6) is readily verified, as the determinant of the observability matrix equals $\overline{\omega}^2$, and therefore the system is fully observable for any arbitrary $\overline{\omega} \neq 0$. The following observer-like filter is now introduced

$$\begin{cases} \dot{\hat{\mathbf{x}}} = A\hat{\mathbf{x}} + L(y - \hat{y}) = (A - LC)\hat{\mathbf{x}} + Ly \\ \hat{y} = C_d\hat{\mathbf{x}} \end{cases} \tag{8}$$

where $\hat{\cdot}$ denotes the estimated value of a variable, while $L = [L_1, L_2, L_3]^T$ is the observer gain vector. It is straightforward to show that the state estimation error $\tilde{\mathbf{x}} = \mathbf{x} - \hat{\mathbf{x}}$ converges asymptotically to 0 when L is designed in such a way that the eigenvalues of A–LC lie in the left-half complex plane; such a condition can always be ensured by a proper choice of L. This filter allows for real-time reconstruction of $\dot{y}(t)$, given by $\hat{\dot{y}}(t)$, from noisy measurements of $y(t)$; this way, it enables voltage control schemes that adapt to the input dynamics. If one uses Equation (8) to compute the frequency-response function from y to $\hat{\dot{y}}$, it is observed that it exactly coincides with that of the ideal differentiator (i.e., $j\omega$) at frequency $\omega = \overline{\omega}$ independently of L, while errors are introduced the further ω deviates from $\overline{\omega}$. In addition, since Equation (8) is strictly proper, high-frequency measurement noise is completely eliminated. In contrast, high-pass filters used to commonly estimate derivatives introduce nonzero phase delays and amplify the high-frequency noise with a nonzero constant factor. In practice, the design of L must be done by ensuring a trade-off between keeping the measurement noise amplification as low as possible (which can be done by keeping the $\mathcal{H}_2$ norm from y to $\hat{\dot{y}}$ in Equation (8) small, requiring small L) and ensuring that the filter provides an accurate estimation of the derivative even for frequencies close to but different from $\overline{\omega}$ (this is truer the faster the eigenvalues of A–LC are, requiring large L). While the main criterion to implement observer-like filter (Equation 8) is to set $\overline{\omega}$ close to the typical working frequency of the EEH, further guidelines for the calibration of L are provided in Section S2, Supporting Information.

The estimated derivative signal $\hat{\dot{y}}(t)$ enables the generation of voltage profiles synchronized with capacitance changes, for both peak-triggered and quadrature control. Peak-triggered control (**Figure 4**A) can be performed by detecting zero crossings of $\dot{y}$. For example, assuming that y has the same monotonicity as the capacitance, changes in $\dot{y}$ from positive to negative provide a trigger condition to start charging. Vice versa, changes from negative to positive provide a trigger condition to start discharging.

For quadrature control (Figure 4B), observer (Equation 8) can be directly used to generate a voltage waveform that varies between 0 and the target voltage V_0 and has 90° phase shift with respect to y. This is achieved by normalizing the estimated derivative $\hat{\dot{y}}$ between ±1, using the observer states and the assumption of harmonic oscillations, namely

$$V(t) = \frac{V_0}{2}\left[1 - \frac{\hat{\dot{y}}}{\sqrt{\hat{y}_{\overline{\omega}}^2\overline{\omega}^2 + \hat{\dot{y}}^2}}\right] \tag{9}$$

where $\hat{y}_{\overline{\omega}} = [0 \quad 1 \quad 0]\mathbf{x}$ is the estimated value of the oscillatory component of y. If $\hat{y}_{\overline{\omega}}$ (and the estimated derivative $\hat{\dot{y}}$) are perfect sinusoids, $\sqrt{\hat{y}_{\overline{\omega}}^2\overline{\omega}^2 + \hat{\dot{y}}^2}$ is a constant, and it equals the amplitude of $\hat{\dot{y}}$, hence providing a normalization factor. Further saturations can be introduced to strictly limit $V(t)$ between 0 and V_0. If $\hat{y}_{\overline{\omega}}$ is not sinusoidal, the derivative estimate is still accurate within a

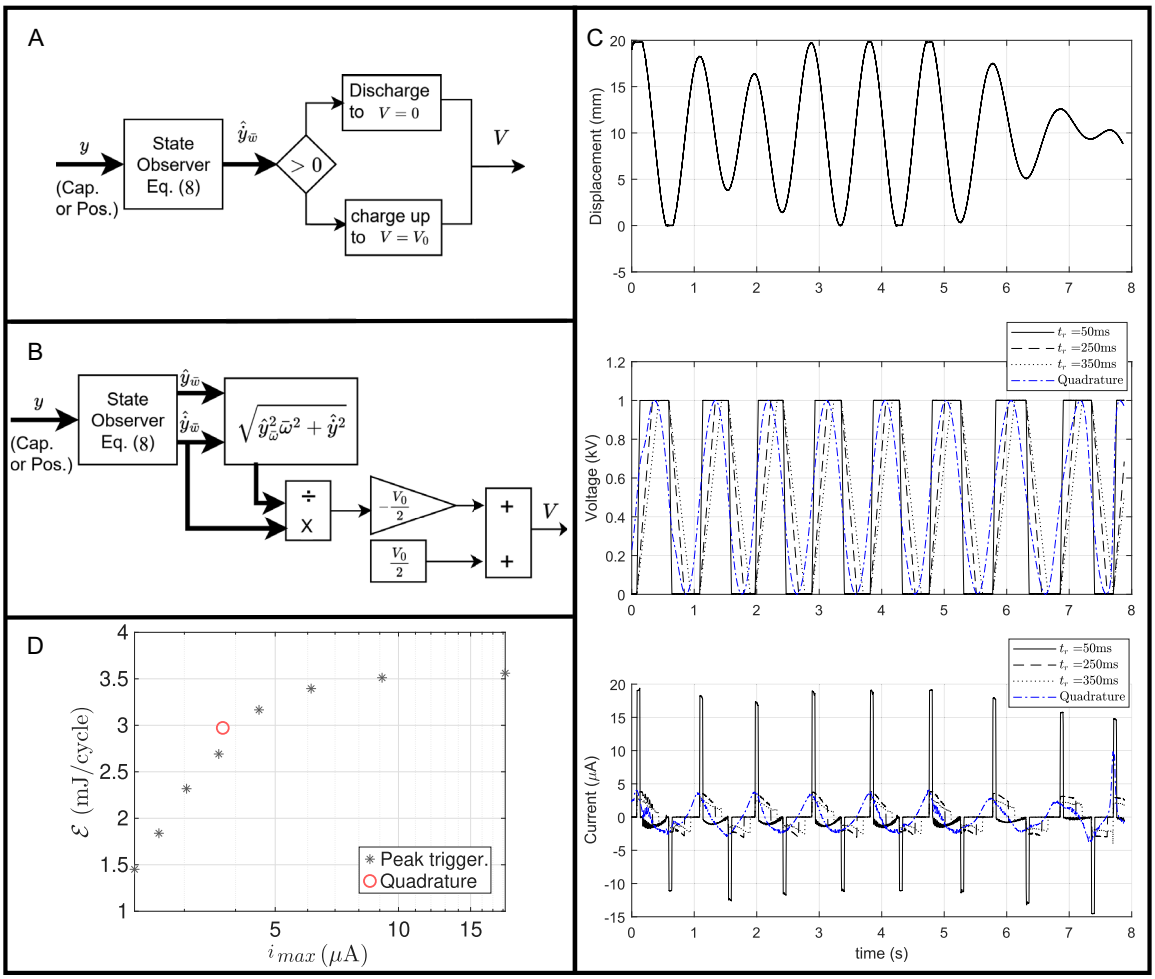

Figure 4. A,B) Closed-loop control logic for real-time implementation of peak-triggered (A) and quadrature (B) control. C) Time series showing a portion of the sample displacement (multichromatic waveform with statistical peak frequency of 1 Hz), voltage, and current for peak-triggered controls with different charging/discharging times and quadrature control. D) Measured generated energy (average per cycle) as a function of the peak current, for peak-triggered and quadrature control.

frequency range around the base frequency, leading to a smooth waveform for $V(t)$ approximating a sinusoid.

Equation (9) does not make use of any prediction of the profile of $y(t)$ into the future, yet it generates a voltage profile that approximately varies between 0 and V_0, provided that the spectral content of y is narrowly distributed around $\bar{\omega}$. In the case of an ideal sinusoidal input y, the resulting voltage signal V is sinusoidal: this corresponds to a limit case for the parametrization provided by Equation (2) for quadrature control, which only covers scenarios with $N \gg 1$. Implementing quadrature controls equivalent to voltage parameterizations with low N would require more sophisticated logic, possibly involving predictions of the system excitation and dynamic evolution.

We implemented the proposed real-time control logic on the DEG samples using the measured displacement as the input control signal y. We applied multichromatic displacement profiles to the DEG, which were generated using a spectral shaping approach. The input displacement signal was synthesized using a band-limited waveform with tunable frequency content. The function was constructed as a sum of sinusoids with randomized phases and amplitudes distributed according to a Weibull power spectral density function. Figure 4C shows the displacement profiles of the DEG for a spectral distribution with Weibull shape factor $k = 10$ and the resulting profiles of current and voltage obtained with different controllers. In the case of peak-triggered controls, increasing the charging time consistently leads to a reduction in peak current. In the case of quadrature control, peak currents on the order of a few microamperes were measured, whereas tens of microamperes were used in tests with steep charging ramps in peak-triggered controls.

The average energy harvested per cycle (Figure 4D) as a function of the peak current has a trend that is consistent with that of monochromatic tests (Figure 3B), which indicates that the quadrature method can provide a higher-energy yield at a given current. At currents of $i_{max} = 3.6\,\mu A$, the energy yield of the quadrature control is 12% higher than that of the associated peak-triggered policy. The advantage of a quadrature control in terms of generated energy over peak current becomes more

conspicuous in the presence of DEG fluctuations with a narrower frequency band (the highest value of the shape factor k), whereas the advantage becomes less evident in the presence of highly harmonic displacements with broad frequency content (Figure S2, Supporting Information). Overall, the results confirm that a quadrature control can offer advantages over traditional peak-triggered controls (in terms of energy generated per current available) even in multichromatic scenarios and without requiring prediction of the system excitation.

2.5. Discussion

The peak-triggered and quadrature control strategies investigated in this study aim to achieve two concurrent objectives: 1) limiting the peak current involved in EEHs operation and 2) providing prediction-free control approaches that do not require a priori knowledge of the mechanical excitation. Limiting peak current and peak power requirements allows downsizing the bidirectional power electronics of EEHs, which represents a technological bottleneck and a significant cost factor.[27] Meanwhile, the ability to achieve high energy conversion without requiring a prediction makes EEHs more easily applicable in the presence of stochastic excitations, which are generally difficult to predict with good accuracy.[34,35] Peak-triggered strategies are inherently prediction free, but their performance drops sharply when the peak current is constrained (Figure 2E). In contrast, quadrature controls can retain a higher-energy yield even under peak current limitations, but they generally require predictions, e.g., the external excitation's phase. Here, we present an approach (Section 2.4) that allows implementing quadrature controls solely based on online measurements or estimation of the EEH capacitance, with no need for prediction.

In the past, intermediate EEH control strategies were presented, in which fixed voltage rates were used for charging/discharging (similar to peak-triggered controls, Figure 1B), with charging (discharging) being anticipated in time with respect to the achievement of maximum (minimum) capacitance (as in quadrature controls, Figure 1C).[24,36] Those strategies bear the potential to achieve higher energy throughput than peak-triggered controls at low peak currents, but they require predictions to determine the timing of charging/discharging.

The control methods discussed in this work are conceived for EEH driven by means of full power electronics, namely bidirectional DC–DC converters,[24,25] which allow controlling the waveform of the applied EEH voltage. Compared to controls based on passive circuits, such as self-priming circuits,[22] synchronous/asynchronous EEHs,[23] or AC-driven generators,[37] which do not require switching components and implement fixed voltage-charge trajectories, the proposed current limiting controls implement trajectories that are close to constant voltage cycles (Figure 2C,D) and potentially lead to larger convertible energy per cycle.

By approximating constant-voltage cycles, the methods discussed in this study are particularly suitable for EEHs working with a constant dielectric gap thickness, in which the working range is upper bound by a constant breakdown voltage. These include comb-drive MEMS generators,[38] in which the capacitance variation is based on a variable overlap between constant-distance parallel plates, and recently developed zipping generators,[13,14] in which capacitance variations are driven by progressive zipping of constant-thickness polymer films. On the other hand, the methods proposed here might be suboptimal for variable thickness EEHs, in which maximum energy conversion is achieved through constant electric field controls. These include DEGs[26] or variable-thickness parallel plate capacitors.[2] Peak-triggered controls can be easily adapted to approximate constant field controls (see, e.g., ref. [24]), by simply adapting the voltage trajectory used between charging and discharging. In contrast, adapting quadrature controls to constant field cycles requires dedicated future studies or case-specific considerations, aimed at guaranteeing that the generated quadrature voltage trajectories comply with maximum electric field constraints. In practice, constant-voltage cycles can still represent a practical option even for variable gap actuators, because the other components in the converters (e.g., switches or insulators) may impose hard constraints on the maximum voltage, and because several EEH topologies feature nonuniform gaps, rendering the application of a uniform electric field unfeasible.[11]

The current limiting strategies discussed here require sensing of the EEH state to trigger charging/discharging or to generate voltage waveforms that are in phase quadrature with the EEH capacitance. While in this study, we have demonstrated that displacement measurements can be used for this purpose, these methods naturally lend themselves to work in combination with capacitance measurements. Possible future developments thus regard the implementation of peak-triggered or quadrature controls in combination with self-sensing strategies, which potentially allow obtaining capacitance measurements concurrently with the EEH voltage driving.[39] Among others, sensing capacitance (rather than displacement of specific EEH parts) could allow applying the proposed control strategies to multiaxis generators, in which capacitance variations are driven by concurrent deformations/motion in different directions.[40]

3. Conclusion

We propose control strategies for EEHs, with the aim of identifying trade-offs between energy generation and maximum current required during operation. Ideal control cycles for EEHs involve charging/discharging the harvesting capacitor in short amounts of time, at the cost of high instantaneous peak powers and currents, much higher than the average cyclic values. High peak currents represent a critical cost factor for power electronics, and are thus especially critical in view of upscaling, such as envisaged applications of electrostatics in large-scale renewable energy harvesting.

We focus on two classes of current-limiting controls for EEHs: peak-triggered controls, which have been used in previous experimental studies on EEHs and rely on event-based finite-time charging/discharging dynamics, and so-called quadrature controls, introduced here, which rely on smooth voltage profiles with a predefined phase shift with respect to the harvester's capacitance. Theoretical analyses, supported by experimental validation on a DEG, show that driving an EEH with a sinusoidal AC voltage leads to 80% of the energy yield of an ideal peak-triggered on–off control (virtually requiring unlimited currents), which is higher

than the energy yield of a peak-triggered control with the same peak current limitation.

While, in principle, generating quadrature voltage waveforms (with given phase shift with respect to the EEH capacitance) might require a priori knowledge of the excitation profile, we propose an online prediction-free implementation of quadrature controls, applicable in contexts where capacitance variations are multichromatic signals with moderate frequency dispersion around a peak frequency. In particular, we use an observer-like filter capable of providing an estimate of the derivative of a control signal (e.g., the EEH capacitance or displacement) and its time-varying amplitude. Such an estimated derivative can be used to generate a normalized control signal (varying within a predefined range with nearly constant amplitude) that can in turn be used as a quadrature voltage waveform in real-time applications.

From the perspective of larger-scale applications of electrostatic harvesting, the results presented in this study can serve as a tool for the design and control of integrated EEH systems, a process that demands identifying trade-offs between energy conversion capability of the harvester and cost/complexity of the power electronics.

4. Experimental Section

DE Sample Manufacturing: The DEG sample was manufactured using a 145 μm-thick silicone membrane provided by SBM Offshore,[16] which was selected as the dielectric material because it is easy to handle and can be conveniently equipped with silicone-based stretchable electrodes, forming a coherent multilayer composite. The effective electrode area in the unstretched state was 30×70 mm. The compliant electrodes were fabricated using a carbon black (CB)–filled silicone composite approach, following a procedure similar to that reported by ref. [41]. In this method, a fine CB powder (Cabot Vulcan XC72) was first dispersed and ball mixed into a volatile solvent (isopropyl alcohol) and then mixed into a two-part silicone elastomer (Dragonskin 30 by Smooth On) to form a homogeneous conductive paste.[41] The resulting conductive mixture was then applied on the elastomer membrane faces by blade-casting it onto the film through a semiautomatic film applicator (AB4400 by TQC with VF1824 applicator) and a thin laser-cut mask (≈280 μm thickness) to create a uniform electrode layer.[41] This composite formulation provided a stretchable electrode material that matched the elastomer's compliance while offering sufficient electrical conductivity.

Experimental Test Rig: The experimental setup used to validate the current limitation strategies is shown in Figure 3A, and consisted of a fully integrated system for real-time actuation, high-voltage driving, and electrical measurement. Deformations of the elastomeric EEH were provided by a DM01-37 × 120 F-HP-R-95 linear motor by LinMot, driven via analog control input. High voltage was supplied using a HAR42-4 high-voltage rack by Hivolt.de equipped with an HA3B3-S amplifier module, fed via an analog input port. Current measurements were performed using the analog output ports of Keithley 6485 picoammeter in the range 0–200 μA, connected in series between the DEG low-voltage electrode and the amplifier's ground.

Data acquisition and control were performed using a Speedgoat real-time target machine. All closed-loop control algorithms, analog signal generation, and data acquisition routines were implemented in MATLAB Simulink Real-Time. Data were acquired at a sampling rate of 20 kHz via the real-time machine.

The DEG was held in place by means of custom 3D-printed PETG clamps, made using a Bambu Lab X1C printer. The use of PETG as the clamp material further enhances friction while avoiding damage to the elastomer. The clamps' geometry was designed to prevent membrane slippage during operation (further details on the clamping mechanism are provided in Figure S1, Supporting Information).

Testing Procedure: For the sake of demonstration, the DEG sample was subjected to a maximum voltage $V_0 = 1$ kV during the tests. This corresponds to an electric field on the order of 10 kV mm^{-1} during operation, which was much lower than the breakdown strength of the used DE material. This voltage allowed to obtain readable currents while limiting the effects of electrical losses, hence allowing to isolate the effects due to capacitance variation.

Open-loop validation tests (Figure 3) were carried out by applying a sinusoidal stroke (1 Hz frequency) of 20 mm to the DEG, synchronized to the commanded motor position. Each test consisted of five repetitions. The generated energy was calculated as the average over the different cycles. The capacitance of the DEG within the operation range used for the test was varied between 520 and 910 pF (measured offline with an impedance analyzer LCX-K107) during open-loop tests. The initial unstretched effective length of the elastomer was 30 mm, with the actuation cycle starting at 33.5 mm (stretch ratio $\lambda \approx 1.12$) and reaching a maximum length of 47.9 mm ($\lambda \approx 1.60$).

Closed-loop tests were performed by applying multichromatic displacement profiles to the DEG through the linear motor. Displacement profiles consisted of variable amplitude oscillations around a motor offset displacement $x_0 = 10$ mm (corresponding to an electrode longitudinal length of 40.7 mm and a stretch $\lambda \approx 1.35$). The displacement profiles were defined as a superposition of harmonics

$$x(t) = x_0 + \sum_{i=1}^{n} \sqrt{2 S_f(f_i) \Delta f}\, \sin(2\pi f_i t + \phi_i) \tag{10}$$

where $\{f_1, \ldots, f_n\}$ are a set of frequencies between $f_1 = 0$ Hz and $f_n = 10$ Hz, spaced apart by $\Delta f = 1/30$ Hz, ϕ_i are random phases, and $S_f(f)$ is a power spectral density function, corresponding to a Weibull distribution. The resulting displacement waveforms were then saturated between 0 and 20 mm. Distributions with a peak frequency of 1 Hz and different values of the shape factor k were used. Higher values of k produce narrower spectra and signals that resemble sinusoids. Each closed-loop control test with multichromatic displacements had a duration of 30 s, corresponding to ≈30 cycles. Implementation of the closed-loop controls was performed using the measured position of the DEG as the control signal $y(t)$, obtained through the magnetic resolver of the linear motor. Control logic for peak-triggered and quadrature control (Figure 4A,B) was implemented in the real-time target machine, using filter (Equation 8) to estimate the derivative $\dot{y}$. The gains used for the observer were chosen based on the guidelines provided in (Section S2, Supporting Information). In the case of quadrature control, the generated voltage signal $V(t)$ was saturated between 0 and V_0 because the normalization introduced in Equation (9) strictly guarantees that the signal stays within the prescribed voltage bounds only in the case of an ideal sinusoidal input signal.

The energy harvested during the cycles shown in Figure 3C,D was computed using the instantaneous current and voltage signals measured across the DEG, by counting the number of generation cycles in each experiment. Integration of the instantaneous power was performed numerically using a trapezoidal method. For open-loop tests with sinusoidal displacement, the peak current (Figure 3B) was calculated as the average of the peak current throughout different cycles. For multichromatic tests (Figure 4D), the peak current was calculated as the average value of the five highest current peaks recorded during the tests, to reject outliers.

Supporting Information

Supporting Information is available from the Wiley Online Library or from the author.

Acknowledgements

The authors would like to thank Emmanuel Taine, from SBM Offshore, who provided the dielectric silicone materials used to build the samples used in the experiments, and the team from 4C Engineering (Inverness, UK) for the fruitful discussions. A.J. gratefully acknowledges the support from the Italian Ministry for University and Research (MUR) through the "Departments of Excellence 2023-27" program (L.232/2016) awarded to the Department of Industrial Engineering. G.M. gratefully acknowledges the support from the European Union under ERC Starting Grant project flEAP (GA: 101163668). G.R. gratefully acknowledges the support of the Deutsche Forschungsgemeinschaft (DFG, German Research Foundation) under grant no. 536978597. Views and opinions expressed are however those of the authors only and do not necessarily reflect those of the Italian Ministry from University and Research, the European Union, the European Research Council, or the Deutsche Forschungsgemeinschaft. Neither MUR, the European Union, the Deutsche Forschungsgemeinschaft nor the granting authorities can be held responsible for them.

Conflict of Interest

The authors declare no conflict of interest.

Data Availability Statement

The data that support the findings of this study are available from the corresponding author upon reasonable request.

Keywords

control, current, dielectric elastomers, electrostatic, energy harvesting

Received: August 18, 2025
Revised: October 31, 2025
Published online:

[1] F. U. Khan, M. U. Qadir, *J. Micromech. Microeng.* **2016**, *26*, 103001.
[2] P. D. Mitcheson, T. Sterken, C. He, M. Kiziroglou, E. Yeatman, R. Puers, *Meas. Control* **2008**, *41*, 114.
[3] D. Skrovanek, D. C. Ludois, in *IEEE Transaction on Energy Conversion*, IEEE, Piscataway, NJ **2024**.
[4] H. Toshiyoshi, S. Ju, H. Honma, C.-H. Ji, H. Fujita, *Sci. Technol. Adv. Mater.* **2019**, *20*, 124.
[5] F. W. Strong, J. L. Skinner, P. M. Dentinger, N. C. Tien, *Reliability, Packaging, Testing, and Characterization of MEMS/MOEMS V*, Vol. *6111*, SPIE, Bellingham, WA **2006**, pp. 23–31.
[6] G. Moretti, S. Rosset, R. Vertechy, I. Anderson, M. Fontana, *Adv. Intell. Syst.* **2020**, *2*, 2000125.
[7] S. Shian, J. Huang, S. Zhu, D. R. Clarke, *Adv. Mater.* **2014**, *26*, 6617.
[8] E. Taine, A. Claverie, F. Caille, S. Seima, N. Fourdilis, J.-M. Hendrikse, R. Boulard, *Electroactive Polymer Actuators, Sensors, and Devices (EAPAD)*, Vol. *13431*, SPIE, Bellingham, WA **2025**, pp. 119–129.
[9] C. Lagomarsini, C. Jean-Mistral, G. Lombardi, A. Sylvestre, *Smart Mater. Struct.* **2019**, *28*, 035003.
[10] M. Liu, R. J. Young, L. Chen, *IEEE Electr. Insul. Mag.* **2025**, *41*, 15.
[11] G. Moretti, M. S. Herran, D. Forehand, M. Alves, H. Jeffrey, R. Vertechy, M. Fontana, *Renewable Sustainable Energy Rev.* **2020**, *117*, 109430.
[12] M. Duranti, M. Righi, R. Vertechy, M. Fontana, *Smart Mater. Struct.* **2017**, *26*, 115014.
[13] R. Yang, M. Yang, P. Fan, T. Lu, T. Wang, *J. Appl. Phys.* **2023**, *134*, 105001.
[14] I. Hess, S. Chamot, B. Boren, P. Musgrave, *Energies* **2024**, *17*, 23.
[15] P. Rothemund, N. Kellaris, S. K. Mitchell, E. Acome, C. Keplinger, *Adv. Mater.* **2021**, *33*, 2003375.
[16] E. Taine, T. Andritsch, I. A. Saeedi, P. H. Morshuis, *Smart Mater. Struct.* **2024**, *33*, 115030.
[17] P. Kerr, *Ph.D. Thesis*, University of Edinburgh, February **2024**.
[18] Wave Energy Scotland, https://www.waveenergyscotland.co.uk/wave-technology/direct-generation/ (accessed: November 12, 2025).
[19] American-made Program, https://www.herox.com/indeep (accessed: November 12, 2025).
[20] A. Kempitiya, D.-A. Borca-Tasciuc, M. M. Hella, *IEEE Trans. Ind. Electron.* **2011**, *59*, 456.
[21] C. Jean-Mistral, T. Vu Cong, A. Sylvestre, *Appl. Phys. Lett.* **2012**, *101*, 162901.
[22] P. Illenberger, K. Takagi, H. Kojima, U. K. Madawala, I. A. Anderson, *IEEE Trans. Power Electron.* **2016**, *32*, 6904.
[23] S. H. Daneshvar, M. Maymandi-Nejad, M. R. Yuce, J.-M. Redouté, in *2019 IEEE Int. Conf. Industrial Technology (ICIT)*, IEEE, Piscataway, NJ **2019**, pp. 349–354.
[24] T. Todorcevic, P. Bauer, J. A. Ferreira, R. van Kessel, in *2013 IEEE ECCE Asia Downunder*, IEEE, Piscataway, NJ **2013**, pp. 461–467.
[25] L. Eitzen, C. Graf, J. Maas, in *2011 IEEE Energy Conversion Congress and Exposition*, IEEE, Piscataway, NJ **2011**, pp. 897–901.
[26] S. J. A. Koh, C. Keplinger, T. Li, S. Bauer, Z. Suo, *IEEE/ASME Trans. Mechatron.* **2011**, *16*, 33.
[27] Q. Yu, C. Liu, R. Li, Z. Pei, D. Guo, T. Mao, X. Shao, *Front. Energy Res.* **2024**, *12*, 1375888.
[28] G. P. Rosati Papini, G. Moretti, R. Vertechy, M. Fontana, *Nonlinear Dyn.* **2018**, *92*, 181.
[29] Z. Xu, J. Tan, H. Chen, K. Di, K. Bao, J. Cheng, X. Xie, S. Zheng, S. Lin, J. Cai, et al., *Nano Energy* **2023**, *109*, 108314.
[30] C. Graf, J. Maas, D. Schapeler, in *Electroactive Polymer Actuators and Devices (EAPAD) 2010*, Vol. *7642*, SPIE, Bellingham, WA **2010**, pp. 362–373.
[31] H. Honma, Y. Tohyama, H. Mitsuya, G. Hashiguchi, H. Fujita, H. Toshiyoshi, *J. Micromechan. Microeng.* **2021**, *31*, 125008.
[32] J. Teng, Z. Cao, C. Ren, J. Xu, X. Guo, X. Ye, *Appl. Energy* **2025**, *388*, 125701.
[33] G. Moretti, M. Duranti, M. Righi, R. Vertechy, M. Fontana, *Electroactive Polymer Actuators and Devices (EAPAD) XX*, Vol. *10594*, SPIE, Bellingham, WA **2018**, pp. 142–154.
[34] M. P. Schoen, J. Hals, T. Moan, *IEEE Trans. Energy Convers.* **2011**, *26*, 627.
[35] G. Thomson, D. Yurchenko, D. V. Val, Z. Zhang, *Energy Convers. Manage.* **2019**, *196*, 1445.
[36] T. Todorcevic, R. van Kessel, P. Bauer, J. A. Ferreira, *IEEE J. Emerging Sel. Top. Power Electron.* **2015**, *3*, 1171.
[37] Z. Xu, K. Bao, K. Di, H. Chen, J. Tan, X. Xie, Y. Shao, J. Cai, S. Lin, T. Cheng, et al., *Adv. Sci.* **2022**, *9*, 2201098.
[38] G.-J. Sheu, S.-M. Yang, T. Lee, *Sens. Actuators A: Phys.* **2011**, *167*, 70.
[39] P. Zanini, G. Rizzello, S. Seelecke, J. Rossiter, M. Homer, *Electroactive Polymer Actuators and Devices (EAPAD) XX*, Vol. *10594*, SPIE, Bellingham, WA **2018**, pp. 315–323.
[40] P. Rolo, J. V. Vidal, A. L. Kholkin, L. N. Alves, *Appl. Energy* **2025**, *396*, 126055.
[41] D. Vignotto, A. Cherubini, I.-D. Srbu, M. Fontana, G. Moretti, *Smart Mater. Struct.* **2024**, *33*, 095022.